Molecular Catalysis 531 (2022) 112709

Contents lists available at ScienceDirect

Molecular Catalysis

journal homepage: www.journals.elsevier.com/molecular-catalysis

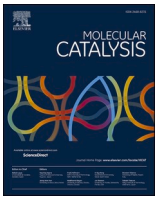

Differentiating supported platinum single atoms, clusters and nanoparticles by styrene hydrogenation

Yuan Zhang [a], Dat T. Tran [b], David Baker [b], Sheng Zhang [c], Tong Wang [c], Sooyeon Hwang [d], Emily Schulman [e], Jiayi Fu [f], Weiqing Zheng [f], Dionisios G. Vlachos [f], Ji Qi [g], Philip Christopher [g], Yang Liu [h], Anatoly Frenkel [h], Dongxia Liu [e,*]

[a] Department of Chemistry and Biochemistry, University of Maryland, College Park, MD 20742, USA
[b] CCDC Army Research Laboratory, FCDD-RLS-DE, 2800 Powder Mill Road, Adelphi, MD 20783, USA
[c] Advanced Science Research Center at the Graduate Center of the City, University of New York, New York, USA
[d] Center for Functional Nanomaterials, Brookhaven National Laboratory, Upton, NY 11973, USA
[e] Department of Chemical and Biomolecular Engineering, University of Maryland, College Park, MD 20742, USA
[f] Department of Chemical and Biomolecular Engineering, University of Delaware, Newark, DE 19716, USA
[g] Department of Chemical Engineering, University of California Santa Barbara, Santa Barbara, CA 93106, USA
[h] Department of Materials Science and Chemical Engineering, Stony Brook University, Stony Brook, NY 11794, USA

ARTICLE INFO

Keywords:
Single atom catalyst
Metal cluster
Nanoparticle
Styrene hydrogenation
Structure sensitivity

ABSTRACT

Supported metal catalysts often consist of metal sites ranging from nanoparticles to subnanometer clusters and single atoms. It remains a necessity to differentiate these sites to guide design of optimal catalysts. Here we report a simple method to assess the distribution of metal active sites in catalyst samples. The method takes the advantage of the structure sensitivity of styrene hydrogenation over titania supported platinum (Pt) catalysts with Pt aggregates varied from single atom to ~1.40 nm nanoparticles. The physicochemical properties were characterized by STEM, XPS, XANES, H_2-TPR and CO-chemisorption measurements. The reactivity of Pt sites was quantified by styrene hydrogenation at ambient conditions. The nanometer-sized Pt clusters have significantly higher activity than Pt nanoparticles, sub-nanometer clusters or isolated single atoms. The relationship between activity and structural/electronic properties of Pt sites influenced by particle sizes was discussed. Similar relationship was found in the carbon supported Pt catalysts.

1. Introduction

Supported noble metal catalysts are extensively used in the petrochemical and pharmaceutical industries to facilitate chemical reaction processes. Due to the natural scarcity and high cost of noble metals, decreasing metal loadings by reducing particle sizes is desired in the heterogeneous catalysis field [1–3]. As a new frontier of this study, single atom catalysts achieving maximized metal dispersion and the potential of atomically-precise active sites are being actively pursued [4–7]. By transiting the metal active sites from nanoparticles to sub-nanometer clusters and then to single atoms, differences in the degree of metal atom aggregation and coordination structures in supported catalysts arise [8–10], which can influence their behavior in catalytic reactions. Therefore, it remains a necessity to identify and differentiate these metal sites and their functionalities, as supported metal catalysts often consist of a mixture of nanoparticles, sub-nanometer clusters and/or single atoms.

Advanced characterization techniques have been used to study the structural and electronic properties of supported metal single atom, cluster and nanoparticle catalysts. For example, high-angle annular dark-field scanning transmission electron microscopy (HAADF-STEM) detects metal particles down to the limit of atomically dispersed species. The metal atoms with different aggregation behavior and particle sizes within the support can be analyzed from this imaging technique [11–13]. X-ray absorption spectroscopy (XAS) probes the electronic state as well as coordination environment of metal catalysts [14]. X-ray absorption near-edge structure (XANES) measures the chemical state of elements of interest by measuring changes in absorption characteristics [15]. First- or even second-shell coordination environments of atoms of interest can be obtained with extended X-ray absorption fine structure

* Corresponding author.
E-mail address: liud@umd.edu (D. Liu).

https://doi.org/10.1016/j.mcat.2022.112709
Received 3 August 2022; Received in revised form 20 September 2022; Accepted 21 September 2022
Available online 24 September 2022
2468-8231/© 2022 Elsevier B.V. All rights reserved.

(EXAFS) spectroscopy [16]. Diffuse reflectance infrared Fourier transform spectroscopy of carbon monoxide (CO) adsorbate (CO-DRIFTS) is another commonly applied characterization technique for supported metal catalysts, which can provide information on local coordination environment, homogeneity, and reactivity of metal active species [17,18].

Catalytic reaction testing is a direct strategy used to examine the performances of supported metal catalysts in selected reaction conditions [19–22]. For example, single atom catalysts have high reactivity in CO oxidation [23,24] and high selectivity in the selective hydrogenation of acetylene groups [25,26], while nanoparticles showed opposite trends in both reactions. The metal clusters showed higher reactivity than the nanoparticles in ethylene hydrogenation [27]. However it has also been reported that the co-existence of single atoms and nanoparticles yields the best activity in the hydrogenation of ketones and aldehydes [28]. It should be noted that a systematic comparison of the supported catalysts with a wide range of metal sizes consisting of nanoparticles, nanometer and sub-nanometer clusters, and single atoms has been rarely reported.

In this work, we employed styrene hydrogenation to identify and differentiate the metal sites and their activities in supported catalysts with different metal particle sizes. The exemplary catalysts are titania (TiO_2) supported platinum (Pt) made by a strong electrostatic adsorption (SEA) approach. The average Pt particle sizes were varied from nanoparticles to sub-nanometer clusters and single atoms by decreasing the Pt loadings during the synthesis. With decreasing particle sizes, the Pt atom reactivity in the styrene hydrogenation reaction shows an increasing then decreasing trend, indicating structure sensitivity of the reaction. The physicochemical properties of the catalysts were analyzed by characterization techniques including HAADF-STEM, X-ray photoelectron spectroscopy (XPS), XANES, temperature programmed reduction by hydrogen (i.e., H_2-TPR) and carbon monoxide (CO) chemisorption. These properties were correlated to the catalytic activity of Pt/TiO_2 catalysts in the styrene hydrogenation reaction. The relationship among structural/electronic properties, reactivity and particle sizes of Pt aggregates was found to be applicable to the carbon supported Pt catalysts.

2. Experimental

2.1. Materials

The titania support (anatase, 99.5% purity) was purchased from U.S. Research Nanomaterial. The Pt precursor, tetraammineplatinum(II) nitrate (TAPN, >99.99% metal basis), was obtained from Alfa Aesar. The ammonia (NH_4OH) solution (28–30 wt.%) were bought from VWR. Styrene (>99.5% purity) stabilized with 10 to 20 ppm 4-tert-butylcatechol was purchased from Acros Organics. Deionized (DI) water was used in the work.

2.2. Catalyst preparation

The Pt/TiO_2 catalysts with Pt concentrations ranging from 0.04 wt.% to 5.00 wt.% were prepared using the SEA method [18]. In a typical synthesis, 0.500 g of as-received TiO_2 powder was dispersed in 50.00 mL of diluted NH_4OH solution that was prepared by mixing 28–30 wt.% NH_4OH and DI water with volume ratio of 1:3. 0.085 g of TAPN was dissolved in 5.00 mL of DI water in a glass vial to form the stock solution. Based on the desired Pt loading in the Pt/TiO_2 catalyst, a certain amount of TAPN stock solution was added into a 25 mL of diluted NH_4OH solution (volume ratio between 28–30 wt.% NH_4OH and DI water = 1:3). The TAPN in NH_4OH solution was then transferred into a syringe and was added into the TiO_2 suspension using a syringe pump (Pump 11, Harvard Apparatus) at a rate of 2 mL/h. Afterwards, the mixture was placed in a convection oven (VWR Sheldon Manufacturing Model, 1350GM Gravity Convection Oven) that was preheated to 343 K. After the sample had fully dried in the oven, it was calcined at 553 K (ramp rate of 5 K/min) for 4 h in a furnace (Thermo Scientific Lindberg/Blue M™ Multipurpose Box Furnaces). The air (Airgas, research grade) flow rate was kept at 50 mL/min during this calcination step. After the sample cooled down to room temperature, it was transferred into a tubular furnace for reduction at 523 K (ramp rate of 5 K/min) for 2 h. The gas atmosphere consisted of diluted H_2 ($5\%H_2/N_2$ mixture) at a flow rate 100 mL/min. The reduced sample was then stored in a desiccator prior to characterization and reaction tests.

2.3. Catalyst characterization

The Pt concentration in each Pt/TiO_2 sample was determined by inductively coupled plasma optical emission spectroscopy (ICP-OES, Galbraith Laboratories). The crystal phase was determined by powder X-Ray diffraction (XRD) patterns recorded using a Bruker D8 Advance Lynx Powder Diffractometer (LynxEye PSD detector, sealed tube, Cu Kα radiation with Ni β-filter). The morphologies of Pt/TiO_2 catalysts with Pt concentrations of 2.00 wt.%, 4.00 wt.% and 5.00 wt.% were observed by STEM measurement with a Thermo Scientific (FEI) Titan Themis S/TEM operating in probe mode at 200 kV with HAADF detector using gun lens 7 and spot size 7. For all other samples, HAADF-STEM imaging was conducted by a Hitachi HD2700C STEM operated at 200 kV and equipped with a probe aberration corrector (spatial resolution ~1 Å). The coordination status of Pt and Ti atoms in the catalysts was probed using a Versaprobe III by Physical Electronics Inc. (PHI) X-ray photoelectron spectrometer. Powders were deposited on carbon tape for sample immobilization in the chamber. X-rays were generated with a monochromated Al Kα anode at 25 W and a beam size of 100 μm. The chamber pressure during analysis was 5×10^{-6} Pa or less. Surveys were performed with a pass energy of 224 eV for each sample, and higher resolution elemental scans were collected with pass energies of 55 eV; both had take-off angles of 45 degrees. A combination of an electron neutralizer and low energy Ar ion neutralizer was used to mitigate surface charging.

The X-ray absorption fine structure spectroscopy (XAFS) measurements at the Pt L3 edge (~11560 keV) were performed on the Quick X-ray Absorption and Scattering (QAS) beamline at the National Synchrotron Light Source (NSLS) II, Brookhaven National Laboratory. XAFS data were collected in the fluorescence mode under ambient condition using a passivated implanted planar silicon (PIPS) detector. The intensity of the incident beam and the absorption of the Pt reference foil were measured with ionization chambers. Athena (0.9.26) software was used for processing XAS data. To obtain good signal to noise ratio all spectra was merged with 80 scans. Attenuated total reflection Fourier transform infrared (ATR-FTIR) spectrum of styrene adsorbate in the catalyst was recorded with a spectrophotometer (Thermo Nicolet NEXUS 670) in the range of 500–4000 cm^{-1}. Each sample was measured with 32 scans at an effective resolution of 2 cm^{-1}.

2.4. H_2-TPR and CO chemisorption measurements

Temperature programed reduction of the Pt/TiO_2 catalyst with H_2 reducing gas (H_2-TPR) was carried out on a Quantachrome Autosorb iQ instrument. A thermal conductivity detector (TCD) was used to record the H_2 consumption in the process. Prior to the measurement, each sample was subjected to a pre-treatment with 40 mL/min N_2 flow (Airgas, Research grade) at 553 K for 2 h. After cooled to 323 K, the gas was switched to 40 mL/min $5\%H_2/N_2$ and the sample was heated to 1173 K at 10 K/min ramp rate and kept at the final temperature for 10 min. A cold trap was used to remove water produced throughout each experiment from the outlet stream to avoid interference with the TCD signal. The chemisorption of CO molecules on the catalyst was measured by pulse titration in the same equipment as the one used in H_2-TPR. The catalyst was first treated in an Ar flow (50 mL/min) at 553 K for 4 h and then cooled down to 523 K. $5\%H_2/N_2$ at a flow rate of 50 mL min^{-1} was

then introduced to reduce the catalyst for 1 h followed by Ar gas purge for 2 h. Afterwards, the sample was cooled down to 303 K in the Ar flowing gas. A series of CO pulses (50 uL in each pulse) were injected with an interval of 5 min until the amount of exit CO pulses reached a steady state value. The CO signal was recorded using a Prima BT Bench Top Process Mass Spectrometers (Thermo Fisher Scientific, winsford U. K. CW7 3GA).

2.5. Styrene hydrogenation

Styrene hydrogenation was used to test the catalytic activity of synthesized Pt/TiO_2 catalysts. Fig. S1 in the Supporting Information shows the experimental setup. In the reaction, 9.00 mL ethanol and 0.050 g catalyst were added into a 50 mL three-neck flask in sequence. The resultant catalyst suspension was sealed in the flask by septa and sonicated for 20 s using an ultrasonic bath (Fisher Scientific FS60). The flask was then placed in a water bath that was preheated to 303 K. A magnetic stirring bar (stirred at 350 rpm) was used to mix the suspension. The center neck of the flask was connected to a condenser. The septum in the right neck was pushed through with a syringe needle to deliver the H_2 gas (50 mL/min, Airgas Ultra High Purity 99.9%) to purge the flask and supply H_2 for the reaction. After purging for 30 min, the styrene solution (0.053 g styrene in 1.00 mL ethanol) was injected into the reactor from the left neck. This moment was recorded as the starting time of the reaction. Reaction mixture was sampled by a syringe equipped with a needle from the left neck of the reactor. After filtering out the solid catalyst particles by syringe filter, the sampled solution was analyzed using a gas chromatography (Agilent 7890A) equipped with a methylsiloxane capillary column (HP-1, 50.0 m × 320 μm × 0.52 μm) and a flame ionization detector (FID). Under the tested conditions, styrene did not have any conversion in the reactor either in the absence of any catalyst or in the presence of TiO_2 support.

The influence of mass transfer limitations on the measured reaction rate data were purposely excluded. Since the catalyst support is nonporous, internal mass transfer limitation is not expected to exist. For the external mass transfer limitation, we eliminated it by running the reaction at high stirring speed. As shown in Fig. S5a in the supporting information, the conversion increased with increasing the stirring speed when the stirring speed was low. After the stirring speed was higher than 300 rpm, the conversion was kept constant. All the reaction data presented in the manuscript were collected at 350 rpm, so the external mass transfer limitation was absent. To test the catalyst deactivation, we recycled the catalyst from reaction mixture by centrifugation. Afterwards, the catalyst was dried in a vacuum oven overnight, and then used for the next cycle of reaction test. As shown in Fig. S5b, the recycled catalyst showed comparable conversions to that of the fresh catalyst, indicating the absence of deactivation in our studied reaction conditions. Eq. (1) was used to calculate the turnover frequency of Pt sites ($TOF_{(Pt)}$, mol s^{-1} [mol Pt]$^{-1}$), where r is the measured reaction rate (mol s^{-1}), N_{Pt} is the quantity of Pt atoms [mol Pt] in each catalyst, and D is the Pt dispersion (%) determined by the CO chemisorption method.

$$TOF_{(Pt)} = r/(N_{Pt} * D) \quad \text{(Eq. 1)}$$

3. Results and discussion

3.1. XRD and STEM analyses of Pt/TiO_2 catalysts with different Pt loadings

The as-prepared Pt/TiO_2 catalysts with Pt concentrations in the range of 0.04 wt.% - 5.00 wt.% were firstly characterized by XRD to understand their crystalline structures. Fig. 1 shows that the XRD peaks of the TiO_2 support are characteristic of anatase phase (JCPDS #75-1537). The average crystalline size is 7.87 nm, calculated from the Scherrer equation using the peak width at half the maximum intensity of the TiO_2 (004) diffraction peak. After the SEA synthesis process, the TiO_2 support maintained the anatase phase, as confirmed by the identical XRD patterns of Pt/TiO_2 samples as that of the TiO_2 support. The broadening in peak width at each diffraction peak indicates that the crystalline size of TiO_2 support was reduced, which could be caused by the corrosive NH_4OH media in the SEA process. The same calculation from the Scherrer equation showed that the average particle size is 6.88 nm, a 12.60% decrease compared to the TiO_2 support prior to exposure to the basic solution. The particle sizes evaluated from the XRD data are comparable to those measured by TEM images. As shown in Fig. S2a, b, the average particle sizes of TiO_2 prior to and after the SEA process were 6.72 and 6.60 nm, respectively. The surface area of the TiO_2 particles (Fig. S2c, d) increased from 185 to 228 m^2/g, accordingly, after the exposure to the basic NH_4OH solution.

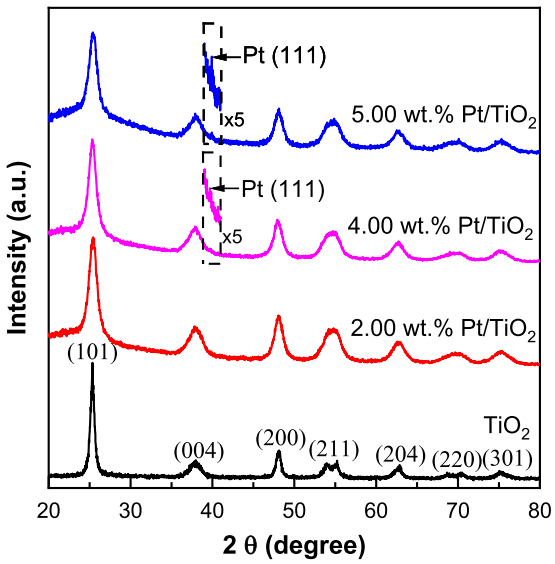

Fig. 1. XRD patterns of TiO_2 supported Pt metal catalysts with Pt concentrations varied from 2.00–5.00 wt.%. The XRD data of TiO_2 support is included for comparison purpose.

It should be noted that all the Pt/TiO_2 samples with Pt concentrations of 0.04–5.00 wt.% have almost identical TiO_2 particle sizes, indicating the consistency of the synthesis process across different Pt/TiO_2 samples. The XRD patterns of Pt/TiO_2 with Pt concentrations lower than 2.00 wt.% were not shown, since they are identical to those of the 2.00 wt.% Pt/TiO_2 sample. The diffraction peak associated with Pt species was not observed until the Pt concentration was increased to 4.00 wt.%. As shown in the XRD patterns of 4.00 wt.% and 5.00 wt.% Pt/TiO_2 samples, the peak at $2\theta = 40^\circ$ is assigned to Pt (111) diffraction, suggesting Pt nanoparticles are formed in these two samples. For all other Pt/TiO_2 samples, the Pt structures are too small to detect in the XRD measurement due to low Pt loading. It should be noted that the elemental composition analysis from ICP-OES shows that no Pt was lost during the SEA process; the Pt concentration in each sample remains nearly the same as the nominal loading used in the catalyst synthesis process (Table S1).

To understand sizes of Pt atom aggregates in the TiO_2 support, HAADF-STEM images were collected, with representative ones shown in Fig. 2. For the 0.04 wt.% Pt/TiO_2 sample, Pt stays as single atoms, as reported previously [18,29]. When the Pt concentration was increased to 0.12 wt.% (Fig. 2a), single atoms and nanoclusters coexist on the TiO_2 support, but the density of Pt nanoclusters was very low. The continual increase in Pt concentrations to 0.25 wt.% (Fig. 2b) increased the density of nanoclusters, but the cluster size did not show any obvious change. In the 0.50 wt.% and 1.00 wt.% Pt/TiO_2 samples (Fig. 2c, d), more Pt clusters are observed, some with slightly larger sizes, as indicated by the circled regions in the images. The further increase in Pt concentration to 2.00 wt.% (Fig. 2e) leads to an increase in density of

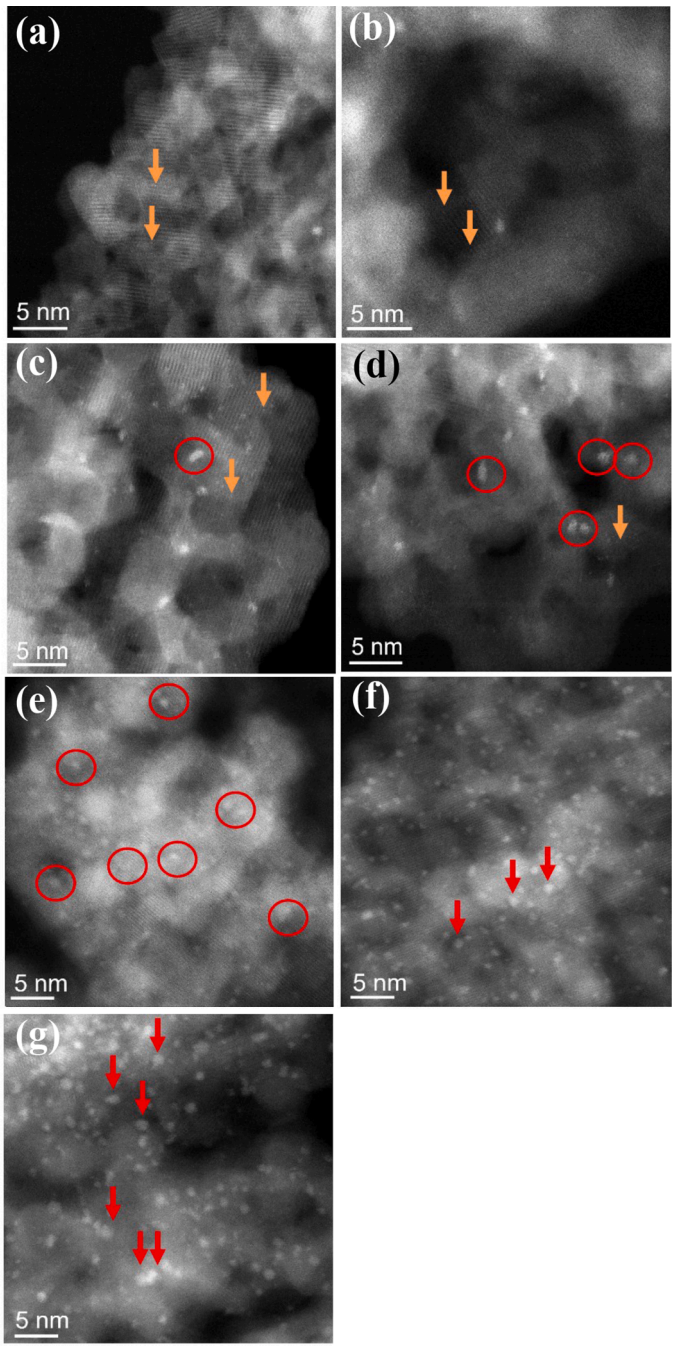

Fig. 2. HAADF-STEM images of Pt/TiO_2 catalysts with Pt concentration of (a) 0.12 wt.%, (b) 0.25 wt.%, (c) 0.50 wt.%, (d) 1.00 wt.%, (e) 2.00 wt.%, (f) 4.00 wt.% and (g) 5.00 wt.%, respectively. Pt single atoms, clusters and nanoparticles are indicated by orange arrow, red circle and red arrow, respectively.

larger Pt clusters, and the sizes of these clusters also increased. We further increased the Pt concentrations to 4.00 wt.% (Fig. 2f) and 5.00 wt.% (Fig. 2g), and both samples showed a high density of large Pt clusters, where some are connected to form even larger particles, as indicated by the red arrows in both images.

The Pt particle size distribution histogram of each Pt/TiO_2 sample was analyzed using statistical analysis of the STEM images. Fig. 3a–g show the particle size data obtained for the samples with Pt concentrations from 0.12 wt.% to 5.00 wt.% in sequence. Due to the resolution cutoff (~0.40 nm) of the STEM instrument, the single atoms and dimers were not included in the size distribution analysis. From direct morphology visualization of the STEM images in Fig. 2, samples with Pt loadings of 0.12 wt.% and 0.25 wt.% have average sizes of 0.72 and 0.75 nm (Fig. 3a, b), respectively. The majority of Pt particles are less than 1.00 nm, which are denoted as sub-nanometer clusters. The increase in Pt loadings to 0.50 and 1.00 wt.% increased the average particle sizes to 1.06 nm and 1.08 nm, respectively, in Fig. 3c, d. The predominant particle sizes in these two samples are close to one nanometer. We defined them as nanometer clusters. For the samples with even higher Pt loadings (i.e., 2.00 wt.%, 4.00 wt.% and 5.00 wt.% in Fig. 3e–g), the average particle size increased monotonically with Pt loadings to 1.28, 1.32 and 1.46 nm in sequence. Most of the Pt atoms in these three samples aggregate into nanoparticles, as the dominant particle sizes are above 1.00 nanometer.

The quantity of Pt atoms in the states of single atoms, sub-nanometer clusters, nanometer clusters and nanoparticles in the Pt/TiO_2 samples were further evaluated from the particle size histograms and total Pt loadings (refer to Section S3 for details). Table 1 summarizes the calculated results. Due to strong metal-support interaction (SMSI) between Pt and TiO_2 support [30], Pt clusters adapt different geometry than the typical hexagonal close-packed cluster on the TiO_2 surface [31,32]. In fact, the structure of sub-nanometer and nanometer Pt clusters was assumed to be planar, as reported previously [29,33]. In this work, the geometry of Pt clusters is calculated based on the work from Zhou et al. [34], in which Pt atoms stay as raft-like, 2-dimensional islands instead of 3-dimensional clusters. For Pt nanoparticles (i.e., larger than 1 nm), Pt reveals a more metallic property, therefore the prediction of Pt nanoparticles with half-octahedrons from Teo and Sloane [35] was adapted. The deduction of Pt atom quantities in the Pt clusters and nanoparticles from the total Pt loading provided the quantity of Pt single atoms. The percentage of Pt single atoms decreases with increasing Pt loading in the Pt/TiO_2 samples. When Pt content is lower than 0.50 wt.%, majority of Pt atoms stay as isolated single atoms. In 0.50 wt.% and 1.00 wt.% Pt/TiO_2 samples, a small percentage of Pt single atoms co-exist with nanometer clusters. In the samples with Pt content above 1.00 wt.%, nearly all Pt atoms agglomerate into clusters and nanoparticles.

3.2. XPS and XANES analyses of Pt/TiO_2 catalysts with different Pt loadings

XPS measurements were performed to study the electronic properties of TiO_2 supported Pt catalysts. In the XPS spectra, the Ti3s line has a satellite peak present in the 70–80 eV binding energy range, overlapping with the Pt 4f XPS spectra, which should be subtracted to obtain precise Pt4f peaks [36]. For this purpose, the XPS spectrum of pure TiO_2 support was recorded under the same measurement conditions. After the intensity of the background line is normalized by the Ti3s line recorded for the Pt/TiO_2 catalysts and pure TiO_2 support, we subtracted the contribution of the lines from the TiO_2 support within the Pt4f XPS peak region in our analysis. Fig. 4 shows the XPS spectra of Pt 4f regions scanned for Pt loading from 0.12 wt.% to 5.00 wt.%. The Pt $4f_{7/2}$ peak shifts from 72.53 eV of 0.12 wt.% Pt/TiO_2 sample to 71.07 eV for the 5.00 wt.% sample, which predominately contains Pt nanoparticles. The peak shift to lower binding energy is attributed to the size and bond geometry change of Pt aggregates on the TiO_2 support. Due to the charge transfer to the support, isolated Pt single atoms on metal oxide have been reported to be cationic [5]. Similarly, small Pt clusters appear to be electron deficient because of the intimate interaction between their two-dimensional flat structure and the support [33,34]. With increasing Pt concentrations, Pt atoms start to form three-dimensional structures [37] where the top layer does not have direct interaction with support. Therefore, the sample shows metallic Pt properties. With increasing Pt loadings in Pt/TiO_2 samples, the Pt aggregate sizes increase as confirmed by structural properties in Figs. 2 and 3 above, and thus the Pt species transitions from cationic into metallic species.

A quantitative analysis of cationic and metallic Pt sites in each Pt/TiO_2 sample was attempted by deconvoluting the Pt $4f_{7/2}$ spectrum into

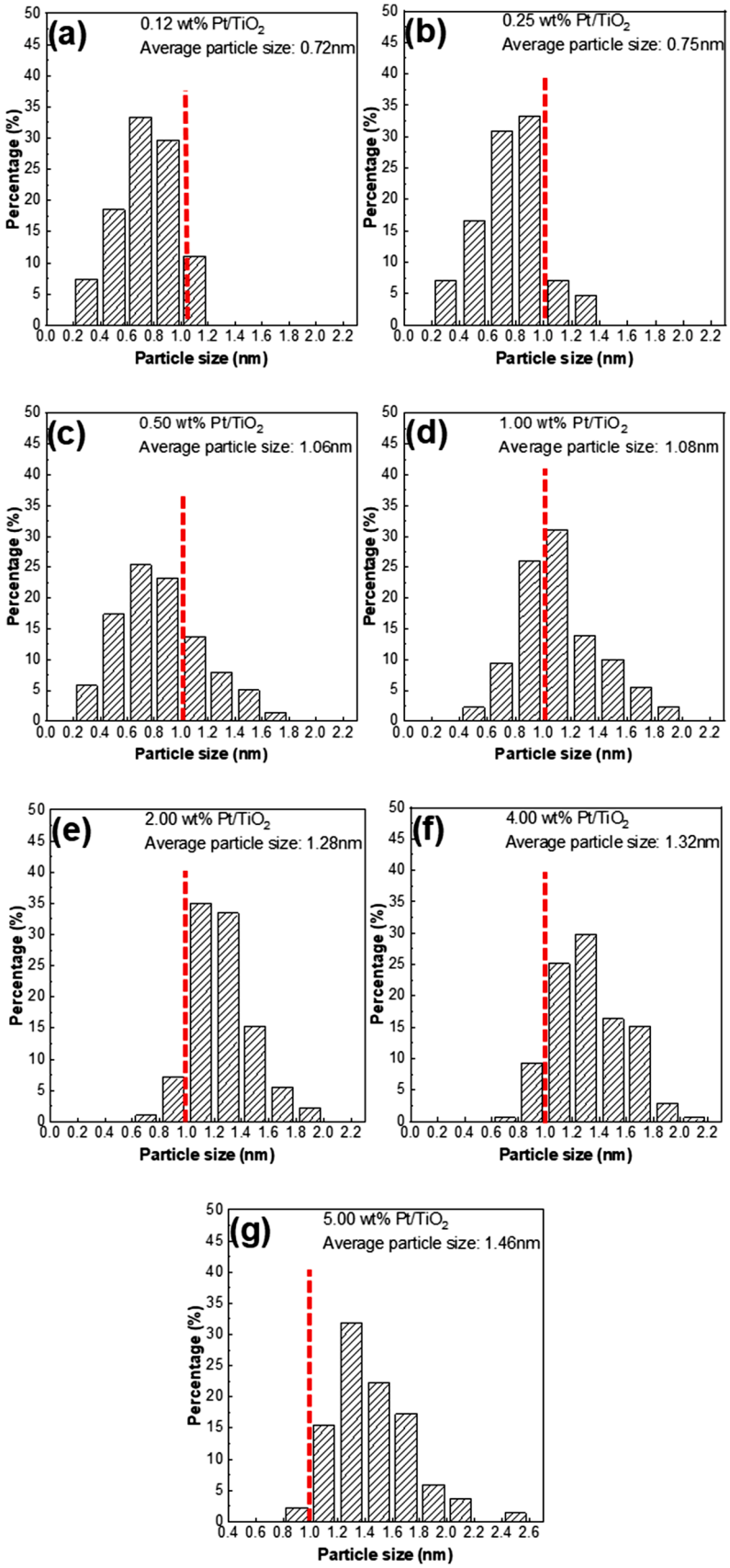

Fig. 3. Particle size distribution of Pt/TiO_2 catalysts with various Pt concentration of (a) 0.12 wt.%, (b) 0.25 wt.%, (c) 0.50 wt.%, (d) 1.00 wt.%, (e) 2.00 wt.%, (f) 4.00 wt.%, and (g) 5.00 wt.%, respectively. ~50 and ~150 particles were counted in (a)-(b) and (c)-(g) respectively. (The vertical red dash line in each figure is used to guide the particle population centered around 1 nm).

Table 1
Activity analysis of Pt sites in isolate single atoms or aggregated nanoclusters and nanoparticles in Pt/TiO_2 catalysts in styrene hydrogenation reaction.

Catalyst (denoted by Pt loading, wt.%)	Pt aggregation state [a]	Pt concentration ([μmol Pt] g^{-1}) [b]	$f_{Pt\text{-}SA}$ (%) [c]	$TOF_{(Pt)}$ (mol s^{-1} [mol Pt] $^{-1}$) [d]	$TOF_{(Pt\text{-}SA)}$ (mol s^{-1} [mol Pt] $^{-1}$) [e]	$TOF_{Pt\text{-}x)}$ (mol s^{-1} [mol Pt] $^{-1}$) [f]
0.04	single atom	2.05	100.0	0.0056	0.0056	-
0.12	subnanometer	6.15	70.5	0.023	0.0056	0.0636
0.25	cluster	12.8	65.7	0.020	0.0056	0.0480
0.50	nanometer cluster	25.6	11.7	0.267	0.0056	0.302
1.00		51.3	2.9	0.460	0.0056	0.474
2.00	nanoparticle	103	0.0	0.446	-	0.446
4.00		205	0.0	0.364	-	0.364
5.00		256	0.0	0.290	-	0.290

[a] Defined from particle histogram data in Fig. 3.
[b] Calculated from Pt loading in each sample.
[c] Calculated by ratio of single atom quantity to Pt loading quantity.
[d] Calculated from Eq. (1).
[e] Evaluated from 0.04 wt.% Pt/TiO_2 and applied to other catalysts that contain both Pt single atoms and aggregates.
[f] Calculated from Eq. (2) by assuming the catalyst contains a mixture of Pt single atoms and Pt single-form aggregates.

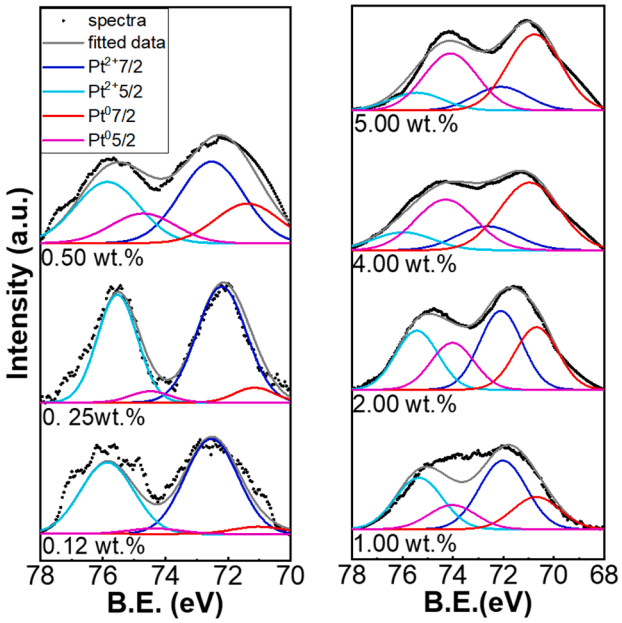

Fig. 4. XPS spectra of Pt 4f of Pt/TiO_2 samples with Pt concentration in the range of 0.04 wt.%-5.00 wt.%. The spectra were calibrated with O1s of anatase TiO_2 at 530.0 eV. (80% Lorentzian-Gaussian peak deconvolution was done using XPSPEAK41).

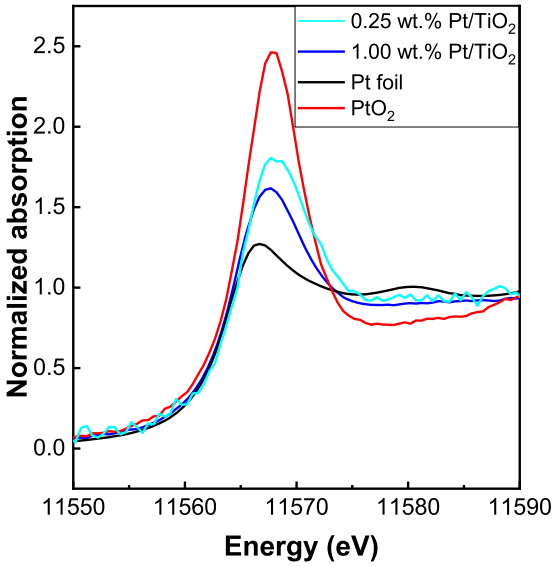

Fig. 5. XANES spectra of 0.25 wt.% and 1.00 wt.% Pt/TiO_2 samples. The XANES spectra of Pt foil and PtO_2 are included as reference.

Pt^{2+} and Pt^0 peaks (details enclosed in Section S2.3). The peak area ratio of each deconvoluted peak based on the total area of both peaks is used to indicate the relative quantity of cationic Pt species. As summarized in Table S2, the Pt^{2+} percentage decreases from 100% in the 0.04 wt.% Pt/TiO_2 sample that contains solely isolated Pt single atoms to 23.78% in the 5.00 wt.% Pt/TiO_2 sample. *Ex-situ* XANES characterization on pre-reduced sample in Fig. 5 also confirmed this conclusion. The oxidation state of Pt metal can be quantitively represented by white line intensity [38]. The overall oxidation state of TiO_2 supported Pt samples lies in between the Pt foil ($Pt_{(0)}$) and PtO_2 ($Pt_{(IV)}$) references. The white line intensity drops with increasing Pt loading from 0.25 wt.% to 1.00 wt.%, which indicates the overall oxidation state of Pt species decreases with increasing particle size.

3.3. Reduction and dispersion of Pt species in Pt/TiO_2 catalysts

To study the reducibility of Pt at different aggregate sizes on TiO_2 support, H_2-TPR was carried out on the Pt/TiO_2 samples with Pt concentration was varied from 0.04 to 5.00 wt.%. As shown in Fig. 6, three major H_2-TPR peaks centered at different temperatures were observed in each sample. The first peak located at ~400 K is associated with the reduction of the PtO_x complex to metallic Pt [39]. The second H_2 consumption peak at ~640 K appears as the largest one among these three peaks, which can be ascribed to the reduction of TiO_2 surface oxygen facilitated by activated hydrogen spillover from Pt [40,41], while the last one at ~940 K is due to the reduction of bulk oxygen of the TiO_2 support [42]. The position of the first reduction peak shifts to lower temperatures with increased Pt loadings in the catalysts, which should be caused by the different Pt aggregation state. For example, the reduction of Pt single atoms in the 0.04 wt.% Pt/TiO_2 sample happened at ~435 K. This reduction peak shifted to ~410 K for Pt sub-nanometer clusters in 0.12 and 0.25 wt.% Pt/TiO_2, ~400 K for Pt nanometer clusters in 0.50 and 1.00 wt.% Pt/TiO_2, and then ~360 K for Pt nanoparticles in Pt/TiO_2 catalysts with loadings above 1.00 wt.%. The stronger interaction between Pt single atoms and the support adds difficulty on H_2 activation on single atoms, and thus shifts the peak to slightly higher reduction temperature. The intensity of this low temperature H_2-TPR peak increases with increasing Pt content in these Pt/TiO_2 samples.

The chemisorption of CO molecules was used to measure the Pt species accessible to reactants in the Pt/TiO_2 catalysts [18,43]. By assuming one CO molecule adsorbs onto one Pt site [44], the number of

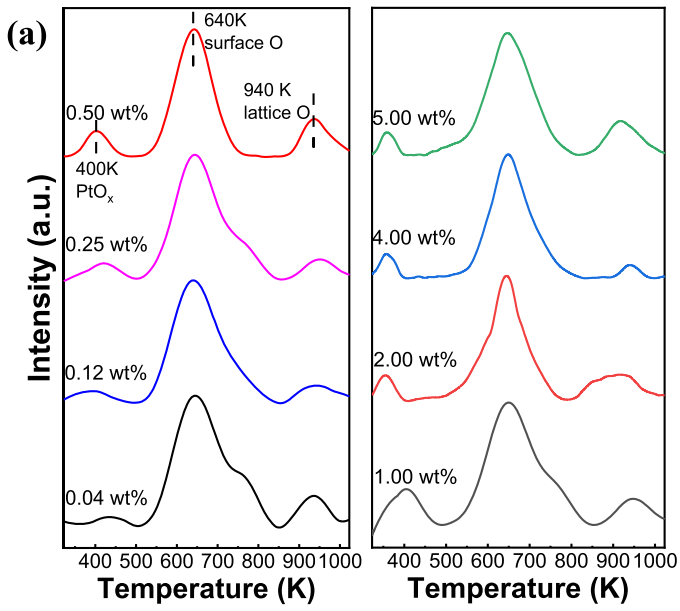

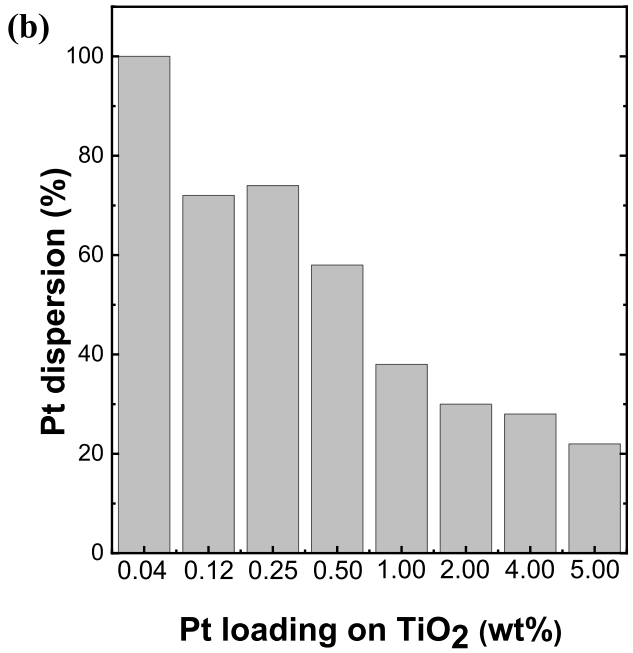

Fig. 6. H_2-TPR profiles (a) and Pt dispersions (b) of Pt/TiO_2 catalysts with various Pt concentrations (0.04 wt.%-1.00 wt.%).

exposed Pt atoms on the catalyst samples and percentages of Pt dispersion (D) can be evaluated. As shown in Fig. 6b, the Pt dispersion in 0.04 wt.% Pt/TiO_2 is nearly 100%, consistent with the atomically dispersed nature of single atoms. The Pt dispersion on 0.12 wt.% and 0.25 wt.% Pt/TiO_2 samples are 72% and 74%, respectively. When Pt loading was increased to 0.50 wt.%, the dispersion dropped to 58%. As a further increase in Pt loading from 1.00 wt.%, 2.00 wt.%, 4.00 wt.% to 5.00 wt.%, the dispersion decreased to 38%, 30%, 28% and 22% in sequence. The CO-chemisorption data indicates different degree of accessibility of Pt sites on Pt/TiO_2 catalysts with different Pt loadings.

3.4. Styrene hydrogenation over Pt/TiO_2 catalysts with different Pt loadings

As a structure sensitive reaction, styrene hydrogenation has been used to discriminate carbon supported metal catalysts with sub-nanometer sizes [45,46]. In this study, we used this reaction to study metal oxide (i.e., TiO_2) supported Pt species with sizes spanning from single atoms, clusters and nanoparticles. We would like to note that all the catalysts were calcined at 553 K in an air flow followed by reduction at 523 K in 5% H_2/N_2 flow prior to the catalysis tests. The effect of SMSI causing encapsulation of Pt species was not expected to influence the catalytic measurements, because SMSI overlayer formation happens at harsher reduction conditions than those explored here, such as ~673 K for metal particles [47] and ~873 K for single atoms [30,48]. All the activity differences measured in the reaction should be directly correlated to the Pt aggregation state that resulted from the SEA synthesis.

Fig. 7a shows the styrene conversions over all the Pt/TiO_2 samples. The increase in Pt content in the catalysts led to a monotonic increase in styrene conversion. The Pt single atom catalyst (0.04 wt.% Pt/TiO_2) had a conversion of ~0.04%, while the Pt nanoparticles in 5.00 wt.% Pt/TiO_2 reached 42.0% conversion. The turnover frequencies (TOF) of these catalysts were extracted from reaction data that the styrene conversion was controlled below 20%. The TOF of these catalysts showed a volcano-shaped trend (Fig. 7b). The 1.00 wt.% Pt/TiO_2 showed the peak reactivity, in comparison to the samples that have lower or higher Pt concentrations. In particular, 0.04 wt.% Pt/TiO_2 sample has a TOF of 5.60 mmol s^{-1} [mol Pt]$^{-1}$, ~82-fold lower than that of 1.00 wt.% Pt/TiO_2. When Pt loadings were increased to 0.12 and 0.25 wt.%, the TOFs were, respectively, increased to 23.09 and 19.73 mmol s^{-1} [mol Pt]$^{-1}$. A significant increase in TOF was observed for the 0.50 wt.% Pt/TiO_2 sample, reaching 266.75 mmol s^{-1} [mol Pt]$^{-1}$. Above 1.00 wt.% Pt loadings, the TOF decreases slowly with increasing Pt content in the Pt/TiO_2 samples. The reactivity of Pt atoms in the catalysts follow the order of nanometer clusters > nanoparticle > sub-nanometer clusters > single atoms. We would like to note that ethylbenzene was the only observed product in the reaction. Therefore, the measured TOFs were solely attributed to the hydrogenation activity of the Pt active sites in the catalysts.

The activity of each category of Pt aggregates (i.e., single atom, sub-nanometer cluster, nanometer cluster and nanoparticle) in the Pt/TiO_2 catalysts was further analyzed by referring to the quantity of isolated Pt atoms and aggregated atoms (Table 1), and the measured overall TOFs in the catalysts. Eq. (2) below was used for the calculation,

$$r = TOF_{(SA)} * N_{Pt-SA} + TOF_{(x)} * N_{(Pt-x)} \quad \text{(Eq. 2)}$$

where r is the measured reaction rate (mol s^{-1}), $TOF_{(SA)}$ is the turnover frequency (mol s^{-1} [mol Pt]$^{-1}$) of Pt single atoms, $N_{Pt\text{-}SA}$ is the quantity of Pt single atoms ([mol Pt] g^{-1}) obtained from the product of percentage of single atoms ($f_{Pt\text{-}SA}$) and catalyst usage quantity (g), $TOF_{(x)}$ is the turnover frequency (mol s^{-1} [mol Pt]$^{-1}$) of Pt atoms in the aggregates (i.e., clusters or nanoparticles), and $N_{Pt\text{-}x}$ is the quantity of active Pt atoms (mol g^{-1}) in these aggregates and calculated by the multiplication of (1- $f_{Pt\text{-}SA}$), catalyst quantity (g) and Pt dispersion (D). For sub-nanometer clusters, nanometer clusters and nanoparticles, "x" is denoted by "sub-C", "nano-C" and "NP", respectively. The reactivity of Pt single atoms was obtained from 0.04 wt.% Pt/TiO_2 samples that were prepared by our group as well as in the Christopher [18] and Vlachos [29] groups. These samples have been characterized to exclusively contain Pt single atoms. In 0.12 wt.% and 0.25 wt.% Pt/TiO_2 samples, Pt single atoms and sub-nanometer clusters coexist. Under the assumption that Pt sites in each category of Pt atom aggregates independently contribute to the reaction, the sub-nanometer Pt clusters have the reactivity of 55.8 mmol s^{-1} [mol Pt]$^{-1}$, ~10 times higher than the Pt single atoms. Similar calculations by using Eq. (2) were conducted to solve for the reactivity of nanometer Pt clusters in 0.50 wt.% and 1.00 wt.% Pt/TiO_2 samples, which showed TOF of 302 and 474 mmol s^{-1} [mol Pt]$^{-1}$, respectively. The Pt nanoparticles in 2.00 wt.%, 4.00 wt.% and 5.00 wt.% Pt/TiO_2 catalysts had the TOFs of 446, 364, and 290 mmol s^{-1} [mol Pt]$^{-1}$ in sequence in the reaction. The TOF of Pt single

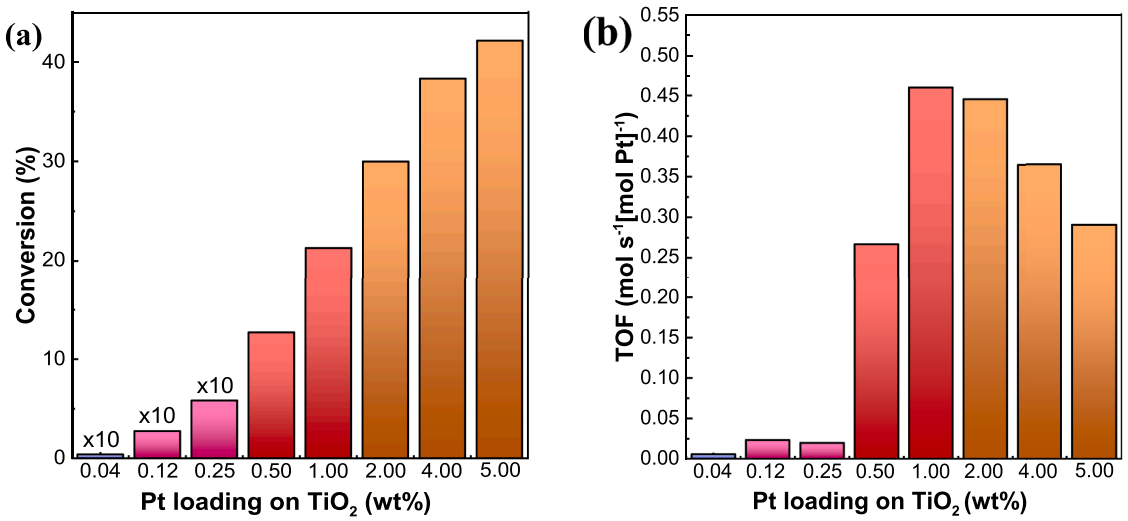

Fig. 7. Styrene conversion (a) and TOF of Pt atoms (b) in styrene hydrogenation over Pt/TiO_2 catalysts with various Pt concentrations (0.04 wt.%-5.00 wt.%). (reaction condition: 303 K, 1 atm pressure, 50 mg catalyst and 0.5 mmol styrene in 10 mL ethanol. Reaction time was 5 min in (a) and conversion of < 20% was used for TOF calculation in (b)).

atoms is ~87 fold lower than that of the nanometer clusters.

Hydrogenation of unsaturated bonds in olefins has been traditionally categorized as a structurally-insensitive reaction because the reactivity does not change with metal particle sizes in the typical range of 1.5–10 nm [27,49–51]. The advent of new catalyst synthesis techniques that produce metal catalysts with sizes of < 1.0 nm recently challenged this conception. For example, the carbon nanotube supported Pt catalysts prepared by atomic layer deposition (ALD) showed that the metal reactivity in styrene hydrogenation changes with Pt particle sizes prepared from different ALD cycles.[44] Similarly, the Pt clusters prepared from the platinum thiolate complexes on Ketjenblack support showed the clusters containing 10 Pt atoms had the maximum reactivity in styrene hydrogenation.[43] A surface science experiment (i.e., under ultra-high vacuum (UHV) and 150 K condition) studied ethylene hydrogenation on MgO supported Pt_n clusters ($n = 8$ to 15, size is smaller than 1 nm). The results showed that the onset for the hydrogenation reaction happened at Pt_{10} clusters and a maximum rate yielded at Pt_{13} clusters [27]. The significant reactivity differences among Pt single atoms, clusters and nanoparticles, and appearance of the maximum reactivity in the 1.00 wt.% Pt/TiO_2 catalyst that was prepared by the SEA synthesis approach in this study seems to be consistent with these previous studies. It should be noted that the predominant Pt cluster sizes in 1.00 wt.% Pt/TiO_2 is ~1.1 nm, about 0.3 nm larger than the Pt/carbon catalysts[43,44] showing the maximum reactivity. This difference could be caused by different supports, as TiO_2 is traditionally viewed as a material capable of providing stronger interaction with the supported metal species [52,53]. In comparison to the ethylene hydrogenation over Pt/MgO catalyst conducted at UHV and low temperature condition [27], we worked with metal oxide supported Pt catalysts at more realistic catalysis conditions. The earlier studies only examined reactivity of Pt clusters [27,45]. while we compared the reactivity of Pt sites ranging from single atoms to clusters and to nanoparticles systematically.

3.5. Relationship between activity and physiochemical properties of Pt/TiO_2 catalysts

The mechanism of structure sensitivity of supported Pt clusters in styrene hydrogenation has not been resolved. Hypothetically, it can be attributed to the electronic and structural properties of supported Pt clusters that have metastable fluxional structures [43,44]. For supported metal catalysts, the electronic and structural properties, and the correlation between these two properties (or one of them) and the catalyst activity have been discussed in several reports [54–56]. The electronic property often refers to: (i) the quantum size effect of metal nanoclusters compared to the bulk metal and (ii) charge transfer between the support and metal. The structural property is often linked to the topology of the active sites (e.g., local shot-range structure containing several atoms or a long-range structure that forms the crystal planes). In our study, given the small sizes of Pt aggregates (i.e., average size less than 1.50 nm, which does not form crystalline plane yet), we considered the electronic property as the charge transfer between the support and metal site and the structural property as the atom topology in the Pt aggregates. The electronic property is thus linked to the Pt atom coordination environment that is reflected by Pt oxidation state that can be determined from the XPS measurements. The theoretical studies showed that a structural transition happens from (quasi-) two-dimensional small clusters to rigid pyramidal clusters with an increasing number of Pt atoms in the catalyst, in which the Pt atoms at the vertices of the pyramidal clusters are electron-rich and can activate carbon double bonds effectively [43]. The experimental evidence for such structural transition is still lacking due to the current instrumentation limitation. This structure change from one to another, anyhow, is related to the Pt aggregate size.

Here we used the percentages of Pt^{2+} species (derived from XPS analyses) and particle sizes (determined from the HAADF-STEM images) of Pt aggregates to represent the electronic and structural properties of Pt/TiO_2 catalysts in the study. As shown in Fig. 8a, the percentage of cationic Pt species decreases with increasing Pt content in the catalysts. Opposite to this trend, the Pt particle size monotonically increases with increasing Pt loading. The intersection of the two plots in Fig. 8a seems to coincide with the peak reactivity of the Pt/TiO_2 catalysts (i.e., 0.50 wt.% Pt/TiO_2 and 1.00 wt.% Pt/TiO_2 samples) in the hydrogenation of styrene (Fig. 8b). For clarity, the intersection region of the plots in Fig. 8a and peak reactivity in Fig. 8b were highlighted by green oval frames. Similar phenomenon was observed in the carbon supported Pt catalysts, as illustrated in Fig. S6 in the Supporting Information.

Styrene hydrogenation has been recognized to involve the surface reaction of co-adsorbed π-bonded ethenyl groups in styrene and dissociated hydrogen [57]. To verify the structural effects on styrene adsorption on the catalyst, ATR-FTIR measurement was carried out on the Pt/TiO_2 catalysts before and after the styrene chemisorption. As shown in Fig. 9a, adsorption on Pt single atoms in 0.04 wt.% Pt/TiO_2 and Pt sub-nanometer clusters in 0.12 wt.% Pt/TiO_2 showed similar

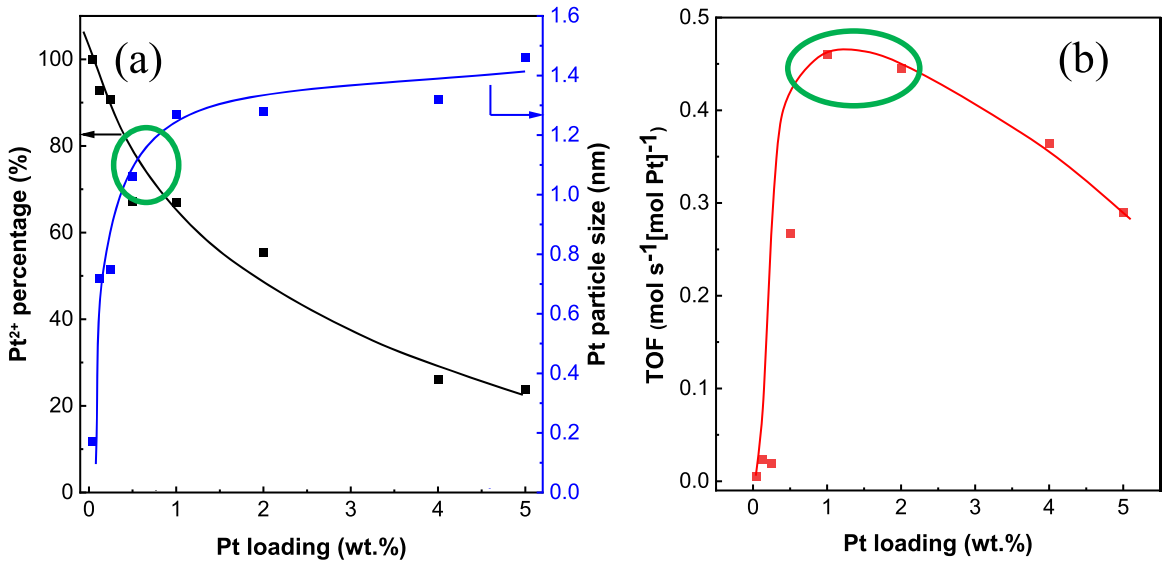

Fig. 8. (a) Structural (indicated by particle size) and electronic (denoted by cationic Pt percentage) properties of Pt/TiO_2 catalysts versus Pt loadings; (b) TOFs versus Pt loadings of Pt/TiO_2 catalysts.

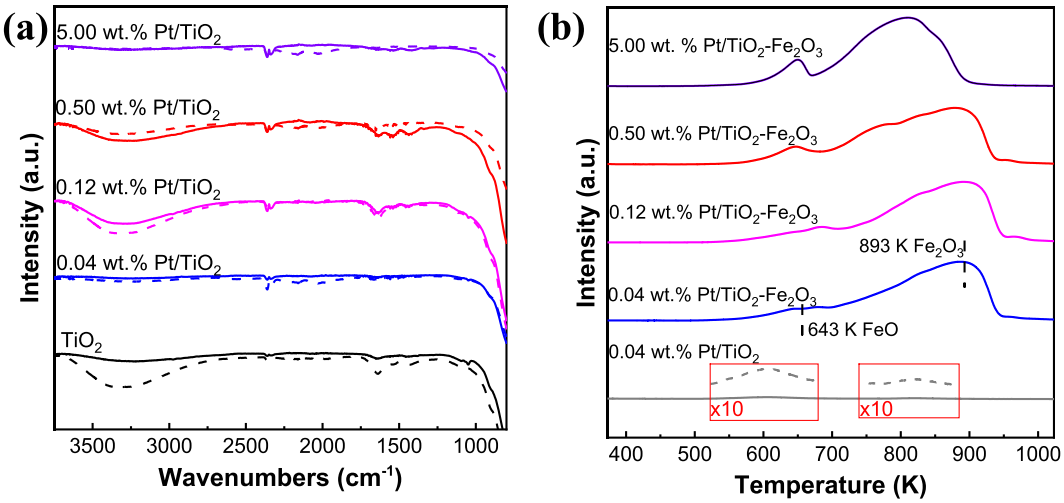

Fig. 9. (a) FTIR of Pt/TiO_2 catalysts with various Pt concentrations (0.04 wt.%-1.00 wt.%) before (dotted line) and after (solid line) styrene chemisorption. (b) H_2-TPR of mixture of Fe_2O_3 and Pt/TiO_2 catalysts with various Pt concentrations (0.04 wt.%-5.00 wt.%).

spectra to that of the TiO_2 support, in which the adsorption of styrene was barely noticeable. In samples containing Pt nanometer clusters and nanoparticles (e.g., 0.50 wt.% and 5.00 wt.% Pt/TiO_2), two peaks (1545 and 1420 cm^{-1}) associated with aromatic C=C bending were observed, indicating the chemisorption of styrene on the samples with larger Pt aggregate sizes. To study hydrogenation property of the Pt/TiO_2 catalysts [58], H_2-TPR of Fe_2O_3 in the presence of Pt/TiO_2 catalyst was measured. As shown in Fig. 9b, two major peaks at ~643 K and ~893 K were detected in the H_2-TPR profiles, which can be assigned to the reduction of Fe_2O_3 to FeO and then to Fe, respectively [59]. The H_2-TPR peaks from the reduction of Pt/TiO_2 catalyst were negligible compared to that of Fe_2O_3 due to the latter's high reducibility. The reduction peaks in the physical mixture of Fe_2O_3 and 0.04 wt.% Pt/TiO_2 or Fe_2O_3 and 0.12 wt.% Pt/TiO_2 stayed at the similar positions, while both peaks moved slightly to lower temperatures when the nanometer Pt clusters in 0.50 wt.% Pt/TiO_2 and nanoparticles in 5.00 wt.% Pt/TiO_2 exist. The data in Fig. 9 suggest the Pt sites with larger aggregation sizes are more effective in enabling the styrene hydrogenation. This conclusion seems to conflict with the highest reactivity achieved in Pt/TiO_2 catalysts with medium Pt loadings (i.e., 0.50 wt.% and 1.00 wt.%), as described in Section 3.4 above. The synergetic effect in the Pt nanometer cluster catalysts might cause the high reactivity. The synergism between noble metal single atoms and nanoparticles has been reported to have the ability to boost the hydrogenation activity of supported metal catalysts [28,60]. Pt single atoms and nanometer clusters coexist in the 0.50 and 1.00 wt.% Pt/TiO_2 catalysts. As the H_2-TPR results indicate hydrogen dissociation preferably happens on metallic nanometer cluster and the activated H atom would spillover towards Pt single atom site to facilitate the hydrogenation of styrene. Whereas on Pt/TiO_2 catalysts with lower or higher Pt loadings, due to the presence of dominant forms of single atoms or large nanoparticles there was trivial synergetic effect, which did not result in high hydrogenation reactivity.

4. Conclusions

In summary, the TiO_2 supported Pt catalysts with different Pt aggregate sizes, i.e., single atoms, sub-nanometer clusters, nanometer clusters and nanoparticles, were prepared by varying Pt loadings on the support using the SEA synthesis process. The structural, electronic, and catalytic properties of these catalysts were studied by a combination of

physicochemical property characterization and styrene hydrogenation reaction. The reactivity of Pt active sites in the form of isolated single atoms is very low. The reactivity increases gently when Pt active sites exist in the sub-nanometer clusters. A significant reactivity increase was observed on the Pt sites in the nanometer clusters. The Pt sites in the nanoparticles showed a slightly decreasing reactivity with increasing Pt particle size in the nanometer scale. The significant variation in reactivity over the Pt sites in single atoms, sub-nanometer and nanometer clusters reflects the structure sensitivity of metastable fluxional catalysts. The maximum reactivity was observed in the Pt/TiO_2 catalyst, in which the predominant Pt cluster size is ~1.1 nm. The physicochemical property characterization showed that the percentage of cationic Pt sites decreases with increasing Pt loadings, while the Pt particle sizes showed an opposite trend. The intersection position of the two plots, i.e., Pt^{2+} percentage versus Pt loading and Pt particle size versus Pt loading, coincides with the Pt/TiO_2 catalysts that have the maximum reactivity. A similar phenomenon was observed in the carbon supported Pt catalysts.

CRediT authorship contribution statement

Yuan Zhang: Methodology, Formal analysis, Writing – original draft. **Dat T. Tran:** Methodology. **David Baker:** Methodology. **Sheng Zhang:** Visualization. **Tong Wang:** Visualization. **Sooyeon Hwang:** Visualization. **Emily Schulman:** Methodology. **Jiayi Fu:** Resources. **Weiqing Zheng:** Resources. **Dionisios G. Vlachos:** Resources. **Ji Qi:** Methodology. **Philip Christopher:** Methodology. **Yang Liu:** Methodology, Formal analysis. **Anatoly Frenkel:** Methodology, Formal analysis. **Dongxia Liu:** Supervision, Formal analysis, Writing – review & editing.

Declaration of Competing Interest

The authors declare that they have no known competing financial interests or personal relationships that could have appeared to influence the work reported in this paper.

Data availability

Data will be made available on request.

Acknowledgments

This work was financially supported by the Catalysis Center for Energy Innovation, an Energy Frontier Research Center funded by the U.S. Department of Energy, Office of Science, Office of Basic Energy Sciences under Award No. DESC0001004. The research is carried out in part at the Center for Functional Nanomaterials, the 23-ID-2 (IOS) beamline of the National Synchrotron Light Source II at Brookhaven National Laboratory, which is supported by the U.S. Department of Energy, Office of Basic Energy Sciences, under Contract No. DE-SC0012704, and at the beamline 7-BM (QAS), which is supported by the Synchrotron Catalysis Consortium, U.S. Department of Energy under Grant No. DE-SC0012335. We also acknowledge the imaging Facility at Advanced Science Research Center of CUNY for instrument use.

Supplementary materials

Supplementary material associated with this article can be found, in the online version, at doi:10.1016/j.mcat.2022.112709.

References

[1] S. Cao, F.F. Tao, Y. Tang, Y. Li, J. Yu, Size-and shape-dependent catalytic performances of oxidation and reduction reactions on nanocatalysts, Chem. Soc. Rev. 45 (2016) 4747–4765.
[2] K. An, G.A. Somorjai, Size and shape control of metal nanoparticles for reaction selectivity in catalysis, ChemCatChem 4 (2012) 1512–1524.
[3] M. Flytzani-Stephanopoulos, B.C. Gates, Atomically dispersed supported metal catalysts, Annu. Rev. Chem. Biomol. Eng. 3 (2012) 545–574.
[4] X.F. Yang, A. Wang, B. Qiao, J. Li, J. Liu, T. Zhang, Single-atom catalysts: a new frontier in heterogeneous catalysis, Acc. Chem. Res. 46 (2013) 1740–1748.
[5] B. Qiao, A. Wang, X. Yang, L.F. Allard, Z. Jiang, Y. Cui, J. Liu, J. Li, T. Zhang, Single-atom catalysis of CO oxidation using Pt 1/FeO x, Nat. Chem. 3 (2011) 634–641.
[6] F. Chen, X. Jiang, L. Zhang, R. Lang, B. Qiao, Single-atom catalysis: bridging the homo-and heterogeneous catalysis, Chin. J. Catal. 39 (2018) 893–898.
[7] J. Liu, Catalysis by supported single metal atoms, ACS Catal. 7 (2017) 34–59.
[8] L. Liu, A. Corma, Metal catalysts for heterogeneous catalysis: from single atoms to nanoclusters and nanoparticles, Chem. Rev. 118 (2018) 4981–5079.
[9] J.M. Thomas, R. Raja, P.L. Gai, H. Grönbeck, J.C. Hernández-Garrido, Exceptionally active single-site nanocluster multifunctional catalysts for cascade reactions, ChemCatChem 2 (2010) 402–406.
[10] S. Vajda, M.J. Pellin, J.P. Greeley, C.L. Marshall, L.A. Curtiss, G.A. Ballentine, J. W. Elam, S. Catillon-Mucherie, P.C. Redfern, F. Mehmood, Subnanometre platinum clusters as highly active and selective catalysts for the oxidative dehydrogenation of propane, Nat. Mater. 8 (2009) 213–216.
[11] T.-Y. Chang, Y. Tanaka, R. Ishikawa, K. Toyoura, K. Matsunaga, Y. Ikuhara, N. Shibata, Direct imaging of Pt single atoms adsorbed on TiO_2 (110) surfaces, Nano Lett. 14 (2014) 134–138.
[12] J. Liu, M. Jiao, B. Mei, Y. Tong, Y. Li, M. Ruan, P. Song, G. Sun, L. Jiang, Y. Wang, Carbon-supported divacancy-anchored platinum single-atom electrocatalysts with superhigh Pt utilization for the oxygen reduction reaction, Angew. Chem. 131 (2019) 1175–1179.
[13] X. He, Q. He, Y. Deng, M. Peng, H. Chen, Y. Zhang, S. Yao, M. Zhang, D. Xiao, D. Ma, A versatile route to fabricate single atom catalysts with high chemoselectivity and regioselectivity in hydrogenation, Nat. Commun. 10 (2019) 3663.
[14] V. Schwartz, D.R. Mullins, W. Yan, B. Chen, S. Dai, S.H. Overbury, XAS study of Au supported on TiO_2: influence of oxidation state and particle size on catalytic activity, J. Phys. Chem. B 108 (2004) 15782–15790.
[15] F. Hilbrig, C. Michel, G.L. Haller, A XANES-TPR study of platinum-rhenium/alumina catalysts, J. Phys. Chem. 96 (1992) 9893–9899.
[16] Z. Zhang, Y. Zhu, H. Asakura, B. Zhang, J. Zhang, M. Zhou, Y. Han, T. Tanaka, A. Wang, T. Zhang, Thermally stable single atom $Pt/m\text{-}Al_2O_3$ for selective hydrogenation and CO oxidation, Nat. Commun. 8 (2017) 16100.
[17] K. Ding, A. Gulec, A.M. Johnson, N.M. Schweitzer, G.D. Stucky, L.D. Marks, P. C. Stair, Identification of active sites in CO oxidation and water-gas shift over supported Pt catalysts, Science 350 (2015) 189–192.
[18] L. DeRita, S. Dai, K. Lopez-Zepeda, N. Pham, G.W. Graham, X. Pan, P. Christopher, Catalyst architecture for stable single atom dispersion enables site-specific spectroscopic and reactivity measurements of CO adsorbed to Pt atoms, oxidized Pt clusters, and metallic Pt clusters on TiO_2, J. Am. Chem. Soc. 139 (2017) 14150–14165.
[19] C.T. Kuo, Y. Lu, L. Kovarik, M. Engelhard, A.M. Karim, Structure sensitivity of acetylene semi-hydrogenation on Pt single atoms and subnanometer clusters, ACS Catal. 9 (2019) 11030–11041.
[20] J.C. Matsubu, V.N. Yang, P. Christopher, Isolated metal active site concentration and stability control catalytic CO_2 reduction selectivity, J. Am. Chem. Soc. 137 (2015) 3076–3084.
[21] J. Resasco, F. Yang, T. Mou, B. Wang, P. Christopher, D.E. Resasco, Relationship between atomic scale structure and reactivity of Pt catalysts: hydrodeoxygenation of m-cresol over isolated Pt cations and clusters, ACS Catal. 10 (2019) 595–603.
[22] Y. Lu, C.T. Kuo, L. Kovarik, A.S. Hoffman, A. Boubnov, D.M. Driscoll, J.R. Morris, S. R. Bare, A.M. Karim, A versatile approach for quantification of surface site fractions using reaction kinetics: the case of CO oxidation on supported Ir single atoms and nanoparticles, J. Catal. 378 (2019) 121–130.
[23] M. Moses-DeBusk, M. Yoon, L.F. Allard, D.R. Mullins, Z. Wu, X. Yang, G. Veith, G. M. Stocks, C.K. Narula, CO oxidation on supported single Pt atoms: experimental and ab initio density functional studies of CO interaction with Pt atom on $\theta\text{-}Al_2O_3$ (010) surface, J. Am. Chem. Soc. 135 (2013) 12634–12645.
[24] D. Kunwar, S. Zhou, A. DeLaRiva, E.J. Peterson, H. Xiong, X.I. Pereira-Hernández, S.C. Purdy, R. ter Veen, H.H. Brongersma, J.T. Miller, Stabilizing high metal loadings of thermally stable platinum single atoms on an industrial catalyst support, ACS Catal. 9 (2019) 3978–3990.
[25] G.X. Pei, X.Y. Liu, A. Wang, A.F. Lee, M.A. Isaacs, L. Li, X. Pan, X. Yang, X. Wang, Z. Tai, Ag alloyed Pd single-atom catalysts for efficient selective hydrogenation of acetylene to ethylene in excess ethylene, ACS Catal. 5 (2015) 3717–3725.
[26] X. Huang, Y. Xia, Y. Cao, X. Zheng, H. Pan, J. Zhu, C. Ma, H. Wang, J. Li, R. You, Enhancing both selectivity and coking-resistance of a single-atom Pd_1/C_3N_4 catalyst for acetylene hydrogenation, Nano Res. 10 (2017) 1302–1312.
[27] A.S. Crampton, M.D. Rötzer, C.J. Ridge, F.F. Schweinberger, U. Heiz, B. Yoon, U. Landman, Structure sensitivity in the nonscalable regime explored via catalysed ethylene hydrogenation on supported platinum nanoclusters, Nat. Commun. 7 (2016) 10389.
[28] L. Kuai, Z. Chen, S. Liu, E. Kan, N. Yu, Y. Ren, C. Fang, X. Li, Y. Li, B. Geng, Titania supported synergistic palladium single atoms and nanoparticles for room temperature ketone and aldehydes hydrogenation, Nat. Commun. 11 (2020) 48.
[29] J. Fu, J. Lym, W. Zheng, K. Alexopoulos, A.V. Mironenko, N. Li, J.A. Boscoboinik, D. Su, R.T. Weber, D.G. Vlachos, C-O bond activation using ultralow loading of noble metal catalysts on moderately reducible oxides, Nat. Catal. 3 (2020) 446–453.

[30] B. Han, Y. Guo, Y. Huang, W. Xi, J. Xu, J. Luo, H. Qi, Y. Ren, X. Liu, B. Qiao, Strong metal–support interactions between Pt single atoms and TiO_2, Angew. Chem. 132 (2020) 11922–11927.
[31] L. Liu, D.M. Meira, R. Arenal, P. Concepcion, A.V. Puga, A. Corma, Determination of the evolution of heterogeneous single metal atoms and nanoclusters under reaction conditions: which are the working catalytic sites? ACS Catal. 9 (2019) 10626–10639.
[32] J. Resasco, L. DeRita, S. Dai, J.P. Chada, M. Xu, X. Yan, J. Finzel, S. Hanukovich, A. S. Hoffman, G.W. Graham, Uniformity is key in defining structure–function relationships for atomically dispersed metal catalysts: the case of Pt/CeO_2, J. Am. Chem. Soc. 142 (2019) 169–184.
[33] Y. Han, C.-J. Liu, Q. Ge, Interaction of Pt clusters with the anatase TiO_2 (101) surface: a first principles study, J. Phys. Chem. B 110 (2006) 7463–7472.
[34] Y. Zhou, C.L. Muhich, B.T. Neltner, A.W. Weimer, C.B. Musgrave, Growth of Pt particles on the anatase TiO_2 (101) surface, J. Phys. Chem. C 116 (2012) 12114–12123.
[35] B.K. Teo, N. Sloane, Magic numbers in polygonal and polyhedral clusters, Inorg. Chem. 24 (1985) 4545–4558.
[36] A. Stadnichenko, D. Svintsitskiy, L. Kibis, E. Fedorova, O. Stonkus, E. Slavinskaya, I. Lapin, E. Fakhrutdinova, V. Svetlichnyi, A. Romanenko, Influence of titania synthesized by pulsed laser ablation on the state of platinum during ammonia oxidation, App. Sci. 10 (2020) 4699.
[37] S.K. Ignatov, A.G. Razuvaev, A.S. Loginova, A.m.E. Masunov, Global structure optimization of Pt clusters based on the modified empirical potentials, calibrated using density functional theory, J. Phys. Chem. C 123 (2019) 29024–29036.
[38] H. Yoshida, S. Nonoyama, Y. Yazawa, T. Hattori, Quantitative determination of platinum oxidation state by XANES analysis, Phys. Scr. 2005 (2005) 813.
[39] C. Zhang, H. He, K.-i. Tanaka, Catalytic performance and mechanism of a Pt/TiO_2 catalyst for the oxidation of formaldehyde at room temperature, App. Catal. B 65 (2006) 37–43.
[40] K. Czupryn, I. Kocemba, J. Rynkowski, Photocatalytic CO oxidation with water over Pt/TiO_2 catalysts, React. Kinet. Mech. Catal. 124 (2018) 187–201.
[41] W.S. Epling, P.K. Cheekatamarla, A.M. Lane, Reaction and surface characterization studies of titania-supported Co, Pt and Co/Pt catalysts for the selective oxidation of CO in H_2-containing streams, Chem. Eng. J. 93 (2003) 61–68.
[42] N.S. de Resende, J.-G. Eon, M. Schmal, $Pt–TiO_2–\gamma$ Al_2O_3catalyst: i. dispersion of platinum on alumina-grafted titanium oxide, J. Catal. 183 (1999) 6–13.
[43] M.J. Kale, P. Christopher, Utilizing quantitative *in situ* FTIR spectroscopy to identify well-coordinated Pt atoms as the active site for CO oxidation on Al_2O_3-supported Pt catalysts, ACS Catal. 6 (2016) 5599–5609.
[44] S. Pisduangdaw, O. Mekasuwandumrong, H. Yoshida, S.-I. Fujita, M. Arai, J. Panpranot, Flame-made Pt/TiO_2 catalysts for the liquid-phase selective hydrogenation of 3-nitrostyrene, App. Catal. A 490 (2015) 193–200.
[45] T. Imaoka, Y. Akanuma, N. Haruta, S. Tsuchiya, K. Ishihara, T. Okayasu, W.-J. Chun, M. Takahashi, K. Yamamoto, Platinum clusters with precise numbers of atoms for preparative-scale catalysis, Nat. Commun. 8 (2017) 688.
[46] J. Li, B. Zhang, Y. Chen, J. Zhang, H. Yang, J. Zhang, X. Lu, G. Li, Y. Qin, Styrene hydrogenation performance of Pt nanoparticles with controlled size prepared by atomic layer deposition, Catal. Sci. Technol. 5 (2015) 4218–4223.
[47] O.S. Alexeev, S.Y. Chin, M.H. Engelhard, L. Ortiz-Soto, M.D. Amiridis, Effects of reduction temperature and metal− support interactions on the catalytic activity of Pt/γ-Al_2O_3 and Pt/TiO_2 for the oxidation of CO in the presence and absence of H_2, J. Phys. Chem. B 109 (2005) 23430–23443.
[48] Z. Wu, Y. Li, W. Huang, Size-dependent Pt-TiO_2 strong metal–support interaction, J. Phys. Chem. Lett. 11 (2020) 4603–4607.
[49] G.C. Bond, Supported metal catalysts: some unsolved problems, Chem. Soc. Rev. 20 (1991) 441–475.
[50] F. Zaera, Key unanswered questions about the mechanism of olefin hydrogenation catalysis by transition-metal surfaces: a surface-science perspective, Phys. Chem. Chem. Phys. 15 (2013) 11988–12003.
[51] F. Zaera, The surface chemistry of metal-based hydrogenation catalysis, ACS Catal. 7 (2017) 4947–4967.
[52] S. Tauster, S. Fung, R.L. Garten, Strong metal-support interactions. Group 8 noble metals supported on titanium dioxide, J. Am. Chem. Soc. 100 (1978) 170–175.
[53] S.Y. Wang, S. Moon, M.A. Vannice, The effect of SMSI (strong metal-support interaction) behavior on CO adsorption and hydrogenation on Pd catalysts: II. kinetic behavior in the methanation reaction, J. Catal. 71 (1981) 167–174.
[54] H. Li, L. Li, Y. Li, The electronic structure and geometric structure of nanoclusters as catalytic active sites, Nanotechnol. Rev. 2 (2013) 515–528.
[55] A. Sápi, T. Rajkumar, J. Kiss, Á. Kukovecz, Z. Kónya, G.A. Somorjai, Metallic nanoparticles in heterogeneous catalysis, Catal. Lett. 151 (2021) 2153–2175.
[56] H. Wang, X.-K. Gu, X. Zheng, H. Pan, J. Zhu, S. Chen, L. Cao, W.-X. Li, J. Lu, Disentangling the size-dependent geometric and electronic effects of palladium nanocatalysts beyond selectivity, Sci. Adv. 5 (2019) eaat6413.
[57] I. Stamatiou, C. Brennan, F.L. Muller, Determination of styrene hydrogenation surface kinetics through detailed simulation of the hydrogen uptake curve, React. Chem. Eng. 4 (2019) 1477–1485.
[58] S. Zhang, Z. Xia, M. Zhang, Y. Zou, H. Shen, J. Li, X. Chen, Y. Qu, Boosting selective hydrogenation through hydrogen spillover on supported-metal catalysts at room temperature, App. Catal. B (2021), 120418.
[59] J. Zieliński, I. Zglinicka, L. Znak, Z. Kaszkur, Reduction of Fe_2O_3 with hydrogen, App. Catal. A 381 (2010) 191–196.
[60] Q. Shen, H. Jin, P. Li, X. Yu, L. Zheng, W. Song, C. Cao, Breaking the activity limitation of iridium single-atom catalyst in hydrogenation of quinoline with synergistic nanoparticles catalysis, Nano Res. (2022) 1–8.